7-2001

Acoustic Radiation from Bowed Violins

Lily M. Wang
Pennsylvania State University, lwang4@unl.edu

Courtney B. Burroughs
Pennsylvania State University, cbb2@psu.edu

Acoustic radiation from bowed violins

Lily M. Wang[a] and Courtney B. Burroughs
Graduate Program in Acoustics, The Pennsylvania State University, P.O. Box 30, State College, Pennsylvania 16804

(Received 31 August 2000; revised 8 March 2001; accepted 9 April 2001)

Near-field acoustic holography (NAH) is applied to visualize the acoustic radiation from bowed violins across a frequency range from 294 Hz to 3 kHz. These visualizations are employed to localize regions of acoustic radiation from surfaces of violins. Three violins were tested: a common student instrument by Scherl and Roth; Hutchins violin SUS295, which has been the subject of many previous investigations; and a Hutchins mezzo violin from the Violin Octet set of instruments, which is longer, broader, and thinner than a standard instrument. The violins were bowed continuously with an open-frame mechanical bowing machine, while NAH measurements were made on four planes surrounding the instrument. Mappings of the acoustic intensity are presented that show locations of maximum radiation at low and high frequencies with a spatial resolution smaller than the acoustic wavelength. Comparisons are made of the radiation patterns between the two conventional instruments and the mezzo violin. Radiation patterns from SUS295 at frequencies near to known modal responses are also presented.
[DOI: 10.1121/1.1378307]

PACS numbers: 43.75.De, 43.75.Yy [RDA]

I. INTRODUCTION

Since its emergence in the sixteenth and seventeenth centuries, the violin has become one of the most loved and subsequently most studied musical instruments. One area that welcomes more study concerns the coupling of the body motion to sound energy radiation from the instrument. Violin mode shapes have been measured and categorized,[1–3] but they are not sufficient to characterize the radiation mechanisms of the instrument. Regions of high surface velocity may not be locations of high-energy output, but rather energy sinks. Furthermore, the sound radiation may have contributions from the air cavity through the *f* holes, not measured by modal analysis.

To understand sound energy radiation requires characterization of the full-field acoustic intensity. This includes magnitude and direction of energy flow at a number of locations and distances from the source for a wide range of frequencies, which amounts to a large quantity of data. A complete study of this kind is lacking in the current literature and has only been feasible in recent years with advances in computer technology. Some previous radiation studies have concentrated on frequency responses. The results, such as Saunders' loudness curves[4] and long-term-average spectra,[5,6] provide pressure magnitude as a function of frequency, but were made only at certain distances or averaged over specific locations around the violin.

Other researchers have measured acoustic intensity from stringed instruments directly, producing vector maps of the energy-flow magnitude and direction. Tro, Pettersen, and Kristiansen[7] used a single microphone with a reference signal to obtain complex pressure measurements, which were converted into intensity, on three planes around a double bass. Only two frequencies, 98 and 230 Hz, were studied, the lower one demonstrating monopole performance, while the higher one showed interesting near-field effects. Tachibana, Yano, and Hidaka[8] presented intensity measurements, as well, on violoncellos to illustrate the sound intensity technique in acoustic near-field. Again, however, the data are available at only a few frequencies and limited to certain planes.

Weinreich and Arnold[9] suggested a more efficient technique for measuring the sound field surrounding a violin using a spherical boom system. Pressure measurements on two spheres could be used with an eigenfunction expansion solution in Hankel functions and spherical harmonics. Solving for the coefficients of the expansion essentially solves for the whole sound field, although concerns were expressed at the time with convergence at small radii. This technique is analogous to that of planar near-field acoustical holography (NAH),[10,11] which Strong and co-workers used on guitars[12] and violins.[13] NAH, which is the basis of measurements taken in this work as well, reconstructs the three-dimensional sound field, including particle velocity and acoustic intensity, from one two-dimensional set of complex pressure measurements. Strong and co-workers sinusoidally excited the instruments at low frequencies (i.e., between 78 and 425 Hz on guitar) and measured two hologram planes, one facing the top plate and the other facing the back plate. Results show the importance of the sound holes and, again, near-field behavior with energy sinks on the source surfaces.

Past studies on violin sound radiation which include both magnitude and direction of energy flow have focused on the lower-frequency regime, but comprehensive investigations of the sound energy radiation from violins at frequencies above 1 kHz have not been performed. When violins are

[a]Current address: Architectural Engineering, University of Nebraska–Lincoln, 200B Peter Kiewit Institute, Omaha, NE 68182-0681; electronic mail: lwang@unl.edu

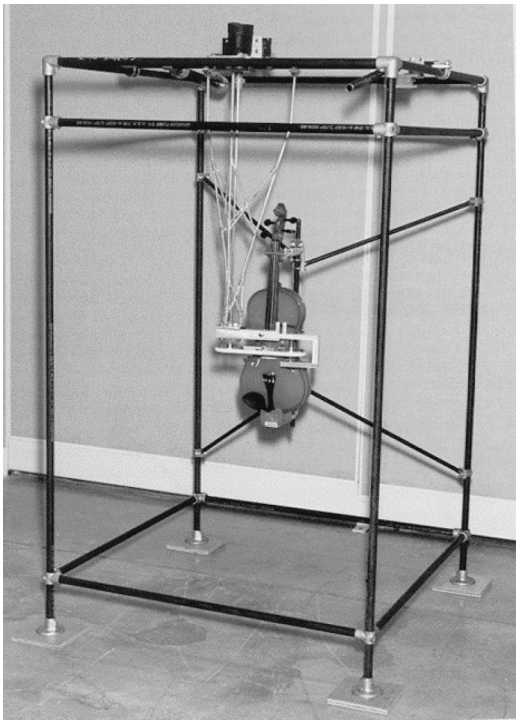

FIG. 1. Frontal view of the open-frame mechanical bowing machine. The violin is held at its neck and tailpiece in the center of the apparatus and driven by a belt sewn with horsehairs on a pulley system.

played, however, much of the sound energy is radiated at frequencies above 1 kHz. The research presented here, therefore, seeks to characterize the radiated sound field when the violin is played at frequencies extending from 294 Hz to 3 kHz, and more specifically, to localize the regions on the violin structure from which significant sound energy originates, with a resolution smaller than the acoustic wavelength. The computational algorithm for producing the surrounding radiated field is based on planar near-field acoustical holography measurements made on four planes which intersect and form a box around the violin.

A further goal of this study has been to determine how the radiation mechanisms differ between instruments of different construction. Hence, the techniques used in this research have been applied to three instruments: a Scherl and Roth full-size violin, rented from a local music store; Hutchins violin SUS295, which has been the subject of many previous experiments, including extensive modal analysis; and a mezzo violin from the Violin Octet instrument family, also made by Hutchins. With its longer and thinner shape, the mezzo violin differs quite significantly in its structure from a standard full-size violin.[14] The effects of the structural changes on the energy flow in the sound field may be established when visually comparing the results from the mezzo violin to those from the other two instruments.

II. METHOD

A. Violin excitation

To excite the violin, a steady-state bowing excitation is favored to simulate true playing circumstances as closely as possible. A custom-designed open-frame mechanical bowing machine has been constructed for this purpose (Fig. 1), and is described in detail in Ref. 15. The bowing machine applies force in a manner similar to the actual excitation of a played instrument, generating a complete set of harmonics as well as torsional motion of the string and coupling between the strings, neck, and fingerboard, which are not initiated by electromechanical excitations at the bridge.[16]

The open frame is constructed from $\frac{1}{2}$ in. black iron pipe shaft tubing. In the center of the frame, the violin rests on a foam pad at the base of the tailpiece and is held loosely at the neck with another foam pad. A driven pulley system running a continuous belt handsewn with horsehairs is placed against the violin strings when excitation is desired. Various bowing parameters may be controlled and measured, including which string is excited, bowing velocity, bow–bridge distance, and bowing force.

The nonlinear interaction between the bow and string strongly excites the motion of the string at the fundamental frequency and harmonics. The present work investigates the radiated fields measured at the frequencies of peak responses, each of which is due to a sum of violin modes. However, the contributions of individual modes to the radiated field are not separated in the analysis as in other studies,[17,18] since the interest lies not in determining the role of each mode but in assessing the combined effect on radiation. At any rate, modal overlap is high at higher frequencies, making continuous excitation of only one mode difficult. At lower frequencies, modal overlap is low, so one may expect modes which have frequencies of resonance close to the frequency of excitation to dominate the response.

B. Three test violins

Two of the three test violins were made by renowned violin maker Carleen M. Hutchins, while the other is a standard model, rented from a local music store. The rented violin is a full-size student instrument manufactured by Scherl and Roth (Model No. R270E4, Serial No. 434104) of mediocre quality, advertised as having a Stradivari design.

Hutchins SUS295 has a long experimental history, including modal analysis[2,19] and monopole radiativity tests,[20,21] both before and after modifications made to the back plate in 1988. A detailed review of experiments which have been performed on the instrument and a specific comparison of SUS295's radiation results from this study with previously documented modal analysis data are presented in Ref. 22.

The third test instrument is a Hutchins mezzo violin, SUS100, from the Violin Octet family. This family, designed by Saunders and Hutchins, consists of eight stringed instruments which are scaled so that the main air and main wood resonances match the frequencies of the middle strings, as is the case with the violin.[23] The mezzo violin was developed as a more powerful ally to the other octet instruments.[14] Compared to standard violins, it has a longer and thinner shape with larger top and back plate areas, which are expected to increase the sound radiation.

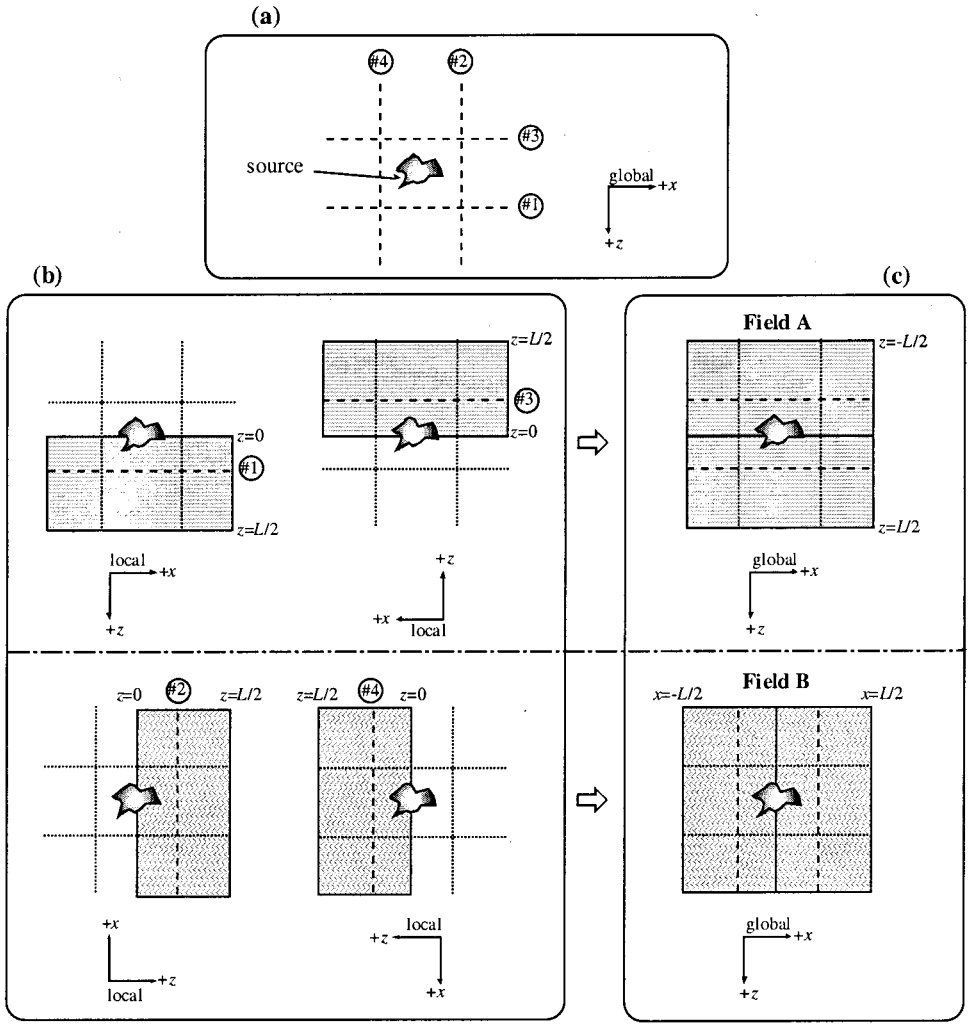

FIG. 2. Multiplanar NAH procedure, drawn in two dimensions: (a) hologram planes 1–4 box the source; (b) each hologram reconstructs a half space in local coordinates; (c) results from holograms 1 and 3 join to form field A, while data from holograms 2 and 4 join to form field B, with global coordinates shown. Finally, fields A and B are combined, either by taking the data in a certain region from the more accurate field or by averaging their values (see Ref. 22).

C. Multiplanar near-field acoustic holography (NAH) technique

To characterize the three-dimensional sound field around any source with high spatial resolution entails a large amount of data. In this study, near-field acoustical holography[10,11] is used to map the three-dimensional acoustic field around the violins from measurements made on four planar surfaces that ''box'' the violin.

Using cylindrical or spherical coordinate systems as the basis for NAH algorithms also produces three-dimensional reconstructions surrounding the source. However, planar NAH with its dependence on fast Fourier transform (FFT) algorithms is easier to implement. Also, for an arbitrary-shaped source such as a violin, the diameter of a sphere or cylindrical hologram would be dictated by the largest dimension of the violin, necessitating measurements at regions which are not in the near field of the violin above certain frequencies. Multiplanar NAH involves boxing the violin, obtaining measurements which are very close to its surface on all sides, thereby providing detailed reconstructions with high spatial resolution.

Four hologram planes of data with dimensions L by L are employed in the measurements. Marked as planes 1–4 in Fig. 2(a), these holograms box the violin and intersect each other. From each hologram, projections to parallel planes are made back towards the source center at $z=0$, and away from the source out to a distance of $z=L/2$, for each local coordinate system shown in Fig. 2(b). The discrete points on each hologram plane and the distances of projection planes are coordinated between all of the holograms, so that all together a lattice is filled with points which are equally spaced over a volume of L by L by L.

Planar NAH has traditionally been used to reconstruct field values only up to the first z plane that intersects the surface of the source. In this study, values at points that remain external to the source but lie on z planes that intersect the source have been reconstructed as well. These values are approximate; an assumption is made that the only contributions to the sound fields at these points are from parts of the source which lie 'beneath' them. This approximation is not inappropriate for the violin, whose shape closely matches the holograms. Additionally, tests of this procedure on simulated known sources showed that the approximations may be acceptable, within 3 dB on average.[22]

No values are reconstructed for points which lie within the surface of the source, since the planar NAH method used is inappropriate for determining the interior sound field. The interior field, moreover, is not the focus of this study. Therefore, as the plane of reconstruction crosses the curved surface of the top or back plate of the violin, values at points that fall

inside the surface are deleted, leaving values only at points that remain outside the surface. It is, therefore, necessary to know where these planes intersect the violin surface. A coordinate measuring machine was used to scan the surfaces of each violin and generate surface coordinates.[22] These coordinates are used not only to determine the surface location when projecting the sound field towards the source, but also to depict the violin surfaces in the visualization software.

After reconstructions from each hologram are processed, the final sound field is composed by first joining the half-space results from holograms 1 and 3, filling a field with planes that extend from $z=-L/2$ to $+L/2$ in the global coordinates shown in Fig. 2(c). Let us call this data set field A. Similarly, half-space results from holograms 2 and 4 are joined, forming a field with planes that extend from $x=-L/2$ to $+L/2$ in global coordinates; this data set is labeled as field B [Fig. 2(c)].

Fields A and B are then combined to form the final radiated sound field result, by taking values only from the more accurate field in some regions and averaging the values in other regions where reconstructions from two planes are expected to be of nearly equal accuracy.[22] A comparison of the accuracy of the multiplanar NAH combination against single planar NAH results has been performed in simulation using a transversely oscillating sphere. Overall, the multiplanar combination proves to be as, or more, accurate than the single planar NAH results in fields A and B.[22]

III. EXPERIMENT

A. Test environment and equipment

Measurements on the Scherl and Roth violin were conducted in a room with concrete walls of size 5.5 m by 7.3 m by 7.0 m. Reflections were minimized by stacking large fiberglass wedges around the apparatus. The experiments on the two Hutchins violins were performed in a semianechoic chamber with interior dimensions of approximately 5.5 m by 6.8 m by 9.3 m. In all cases, the bowing machine was placed on a concrete floor, which was covered with 2-in.-thick foam in the immediately surrounding area.

Four planes of hologram data were measured around each violin, parallel to the four sides of the apparatus frame. Since the recommended aperture size for planar holograms is at least twice the size of the source in each dimension, a hologram of 1.2 m by 1.2 m was chosen. Hologram measurements were made for the Scherl and Roth instrument over a 30 by 30 grid of points evenly spaced at 4 cm, while bowing the open A string. Thus, wave numbers for the first three partials up to 1320 Hz could be resolved. For the tests run on SUS295 and the mezzo violin, measurement positions were 1 cm apart, filling a 120 by 120 point hologram aperture; consequently, wave numbers for frequencies up to 3 kHz have been resolved. The open D and A strings were tested for SUS295, while only the open A string was measured for the mezzo violin, so this frequency range covers at least the first six partials for each string studied. Near-field holograms for the three violins were measured at distances of 1–4 cm away from the nearest exterior point on the surface of the violin; thus, for the highest measurement frequency of 3 kHz, most measurements were made at a distance of less than a quarter of a wavelength.[22]

TABLE I. Bowing parameters maintained during hologram measurements for the listed violins and string excitations.

Violin and string excitation	Bow speed (m/s)	Bow–bridge distance (m)	Bow force (N)
Scherl and Roth, open A	0.35	0.03	0.6
SUS295, open A	0.35	0.03	1.0
SUS295, open D	0.35	0.03	0.8
Mezzo violin SUS100, open A	0.35	0.03	1.0

A linear array of 15 electret microphones was used to obtain the complex sound pressure measurements. The diameter of each transducer is 1 cm; accordingly, the microphone size was much smaller than the wavelength for the highest frequency of 3 kHz, where $\lambda=11.4$ cm. The compact microphones were aligned vertically and attached to a one-dimensional positioning slide, situated horizontally on custom-built legs. While the array was moved to different positions in the horizontal direction by a computer-controlled stepper motor, its vertical placement was adjusted manually to eight positions, providing measurement locations that were vertically 1 cm apart. The positioning slide was kept at a fixed location in the testing rooms, while the bowing machine was rotated for each hologram measurement. A condenser microphone was clamped to the lower of the top bars on the bowing machine frame, facing the top plate of the violin. The signal from this microphone provided a phase reference for data collected by the traversing array.

The 16 channels of data were digitally acquired through a simultaneously sampling 16 bit analog-to-digital (A/D) board, mounted in a PC computer which ran the Hewlett Packard Visual Engineering Environment (HPVEE) software program. A low-pass filter with cutoff at 5 kHz was applied. Before measuring any hologram data, the electret microphones and their signal paths were calibrated relative to the reference microphone. Two standing-wave tubes were used to cover the frequency range from 100 Hz to 5 kHz.[22]

B. Hologram acquisition and field reconstruction

Prior to the start of each hologram measurement, the violin was tuned, and the various bowing parameters were adjusted to desired values within typical ranges.[24,25] Table I lists the parameters used for each violin test. Since the parameters were not the same between violins, comparisons between absolute levels are not made. Relative magnitudes are contrasted, however, since the violin behaves as a linear system.

A program written in HPVEE coordinated the acquisition of the hologram data. At each position, time signals from the 16 channels were simultaneously sampled for 1 s at 10 kHz for the Scherl and Roth tests, and at 15 kHz for the tests on the other two instruments. No additional averages were taken, since the data were deterministic and demonstrated sufficiently high spectral levels at the fundamental and harmonic frequencies. The signals from the reference microphone and each electret microphone were constantly monitored with a frequency analyzer to ensure the stability of the signal level.

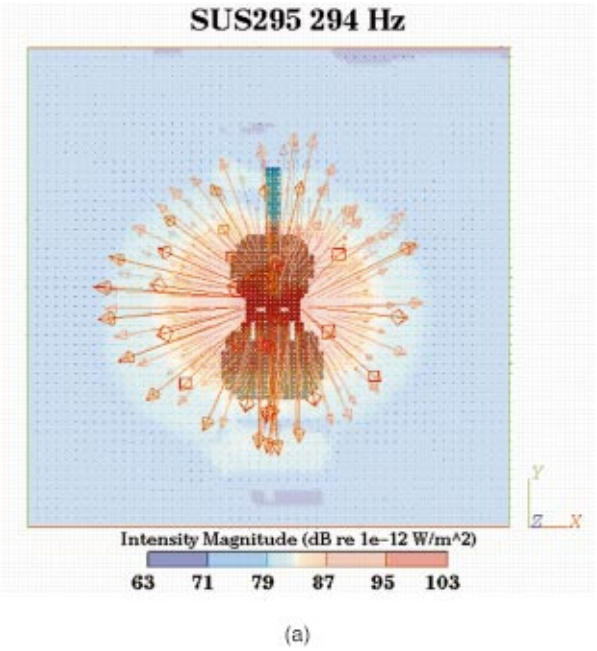

FIG. 3. NAH reconstructed intensity field for violin SUS295 at 294 Hz: (a) facing the top plate and (b) facing the back plate. The plotted data are from the closest local z plane that does not intersect the violin surface. The three-dimensional intensity vectors are shown, while the intensity vector magnitudes are denoted by color.

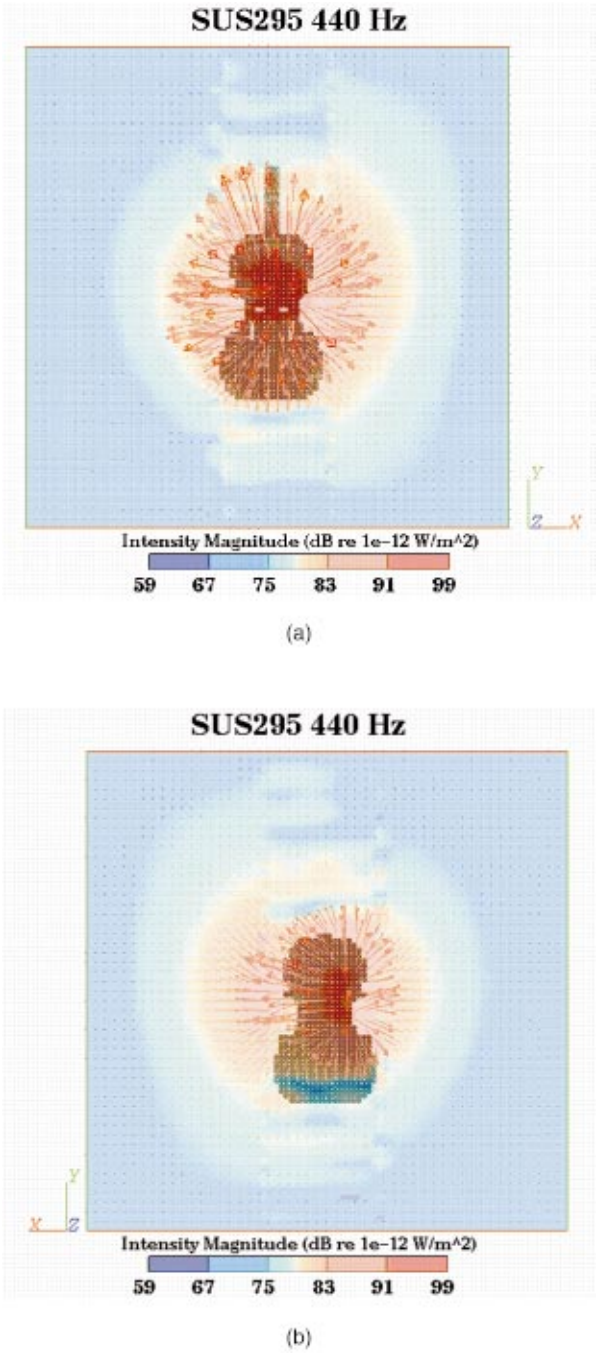

FIG. 4. NAH reconstructed intensity field for violin SUS295 at 440 Hz: (a) facing the top plate and (b) facing the back plate. The plotted data are from the closest local z plane that does not intersect the violin surface. The three-dimensional intensity vectors are shown, while the intensity vector magnitudes are denoted by color.

HPVEE processed the raw time signals at every position, first by applying a Hanning window, then taking an FFT to produce results in the frequency domain. Calibrations for amplitude and phase were applied. The resulting data demonstrated signal-to-noise ratios of at least 30 dB at the frequencies of each partial for each bowed string up to 3 kHz.

A program in *C* was used to consolidate selectively the data from all of the spectra files into the spatial holograms for each of the partial frequencies between 100 and 3000 Hz. A discrete implementation of planar NAH coded with MATLAB and *C* was subsequently applied for reconstruction in local coordinates, producing results for the pressure magnitude and the active intensity in three dimensions.[22] The N by M point hologram is spatially windowed with a broad Tukey window[26] and zero-padded to at least twice the aperture size in MATLAB; then, the *C* code Fourier transformed the spatial data to the wave-number domain, multiplied by the appropriate Green's function ''propagator'' for the desired reconstruction distance, applied an additional k-space window for inverse reconstruction, and finally, inverse transformed back to the real domain. The reconstructions were

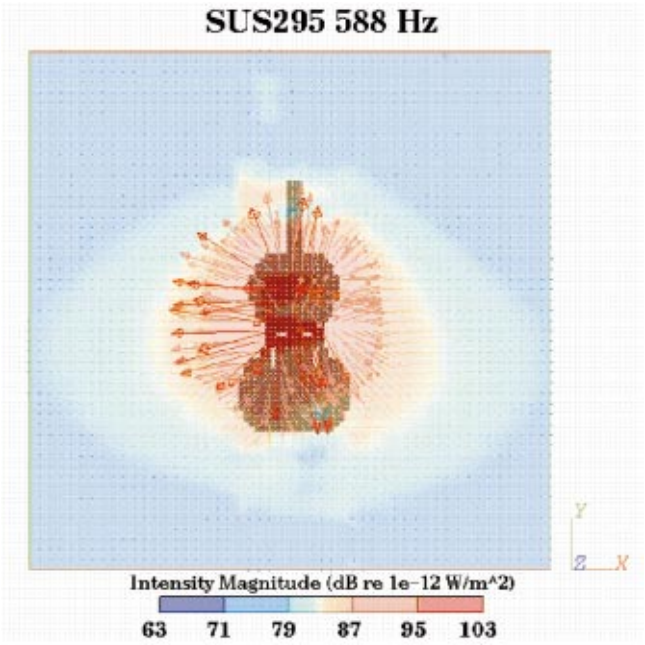

(a)

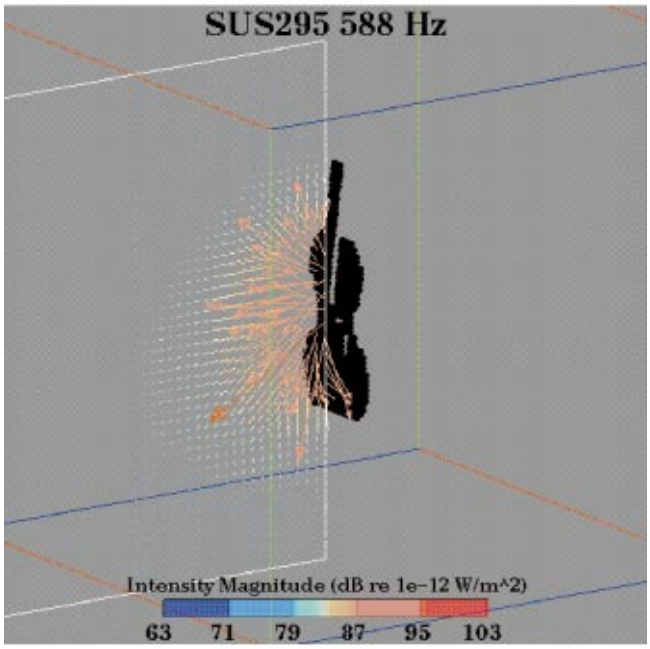

(b)

FIG. 5. NAH reconstructed intensity field for violin SUS295 at 588 Hz: (a) facing the top plate and (b) vectors on a slice through the field showing near-field effects. The three-dimensional intensity vectors are shown, while the intensity vector magnitudes are denoted by color.

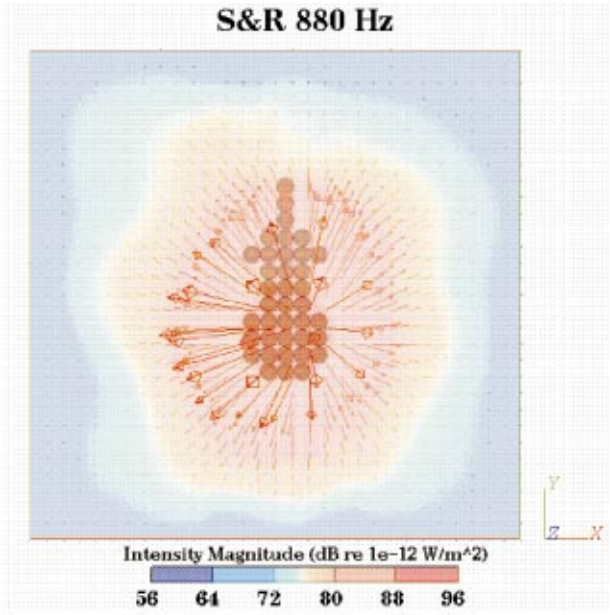

(a)

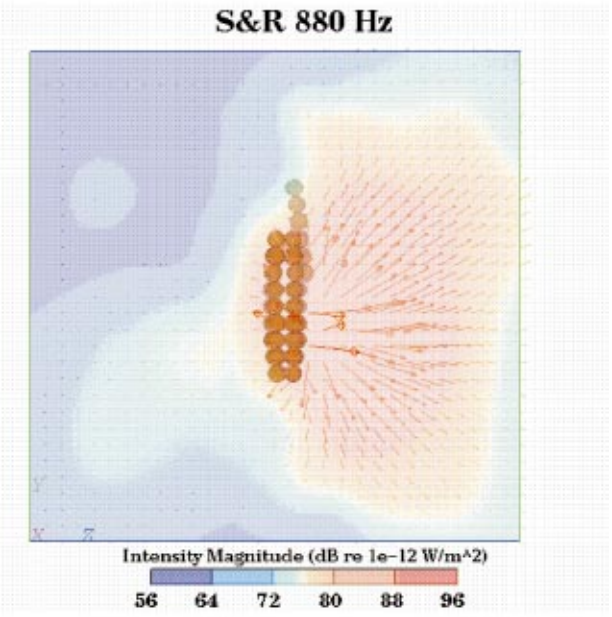

(b)

FIG. 6. NAH reconstructed intensity field for the Scherl and Roth violin at 880 Hz: (a) facing the top plate and (b) facing the bass bar side. The plotted data are from the closest local z plane that does not intersect the violin surface. The three-dimensional intensity vectors are shown, while the intensity vector magnitudes are denoted by color.

accomplished from the hologram onto parallel planes separated by a distance equal to the spacing between measurement points, filling a lattice of discrete points evenly spaced at 4 cm for the Scherl and Roth violin, and 1 cm for the other two violins. Planes of reconstruction from each hologram extended from the local $z=0$ center plane to $z=L/2$, where L is the size in one dimension of the reduced aperture (1 m).

After the half-space reconstructions were accumulated, they were combined according to the multiplanar NAH procedure reviewed above. Due to variations in bowing parameters and the situation of the bowing machine in the testing rooms, the absolute values from the four half-space reconstructions were not consistent in overlapping regions. It was clear from visual study, however, that the data in these areas did have the same relative values within each field. Thus, the half-space reconstructions were normalized to each other, prior to the combination procedure, resulting in an average magnitude difference of 1 dB in overlapping corners across

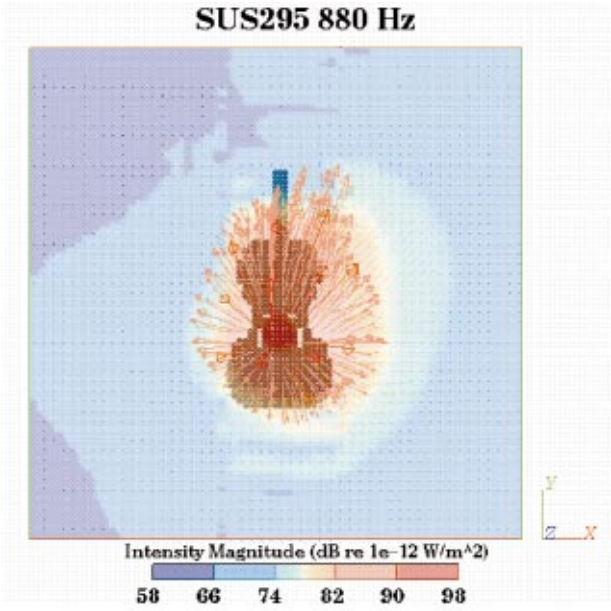

(a)

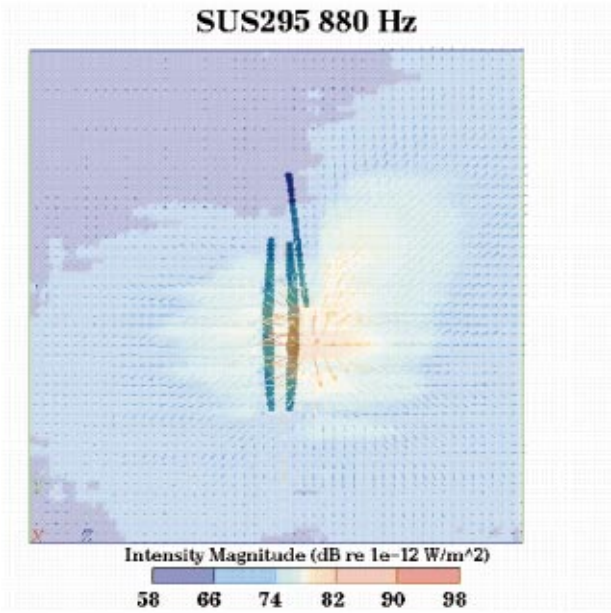

(b)

FIG. 7. NAH reconstructed intensity field for violin SUS295 at 880 Hz from excitation of the open A string: (a) facing the top plate and (b) facing the bass bar side. The plotted data are from the closest local z plane that does not intersect the violin surface. The three-dimensional intensity vectors are shown, while the intensity vector magnitudes are denoted by color.

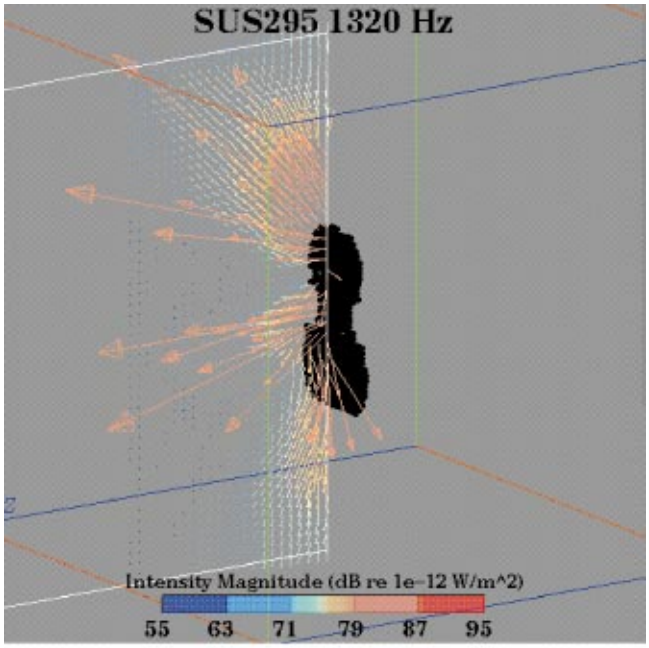

(a)

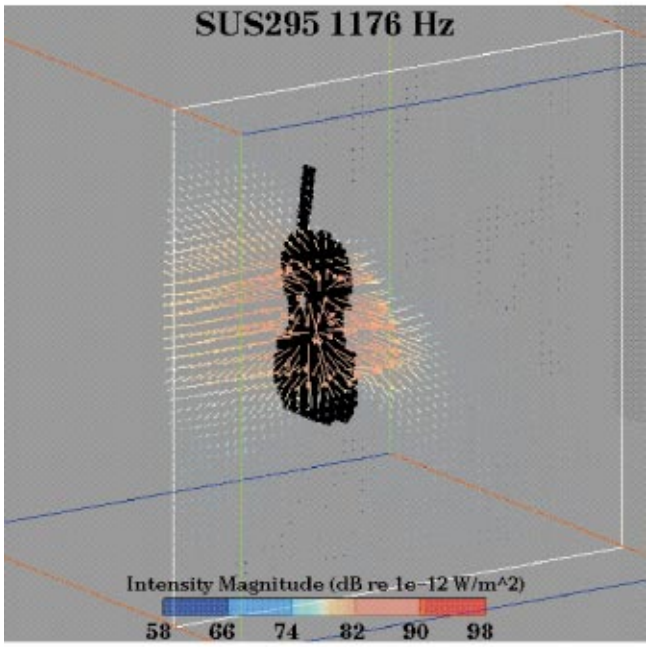

(b)

FIG. 8. Slices through the NAH reconstructed intensity vector fields for violin SUS295 at (a) 1320 Hz, showing directions of energy radiation not normal to the violin, and (b) 1176 Hz, showing vectors which curve around the edges of the violin. The three-dimensional intensity vectors are shown, while the intensity vector magnitudes are denoted by color.

the frequencies studied.[22] The pressure and active intensity results were finally visualized using the software Application Visualization System (AVS).

IV. RESULTS

Examination of the radiated sound field in terms of the active intensity vectors provides knowledge of the location of energy sources on the violin, as well as the direction of energy radiation from the instrument. For both the Scherl and Roth and SUS295 violins, what is most apparent across all frequencies studied is the dominance of the top plate as a radiator of sound energy (Figs. 3–10). The vectors which are greatest in magnitude always originate from the top plate, producing lobes radiating strongly outwards. Even at the lowest frequencies which demonstrate omnidirectional behavior,[15] such as 294, 440, and 588 Hz for SUS295, most of the intensity vectors originate from the top plate.

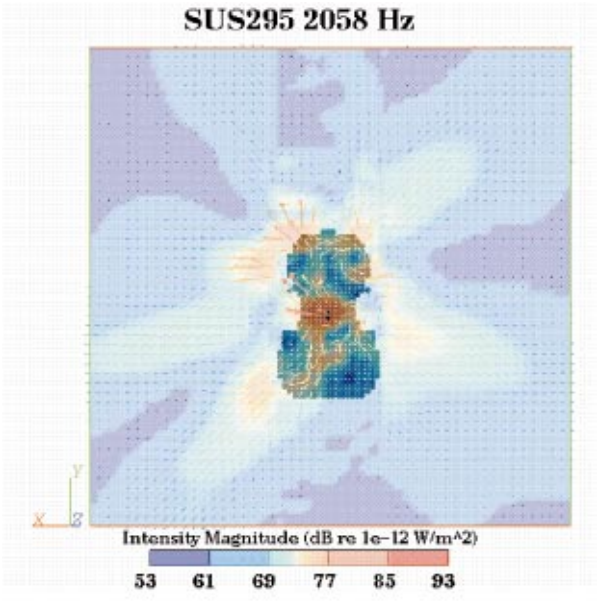

(a)

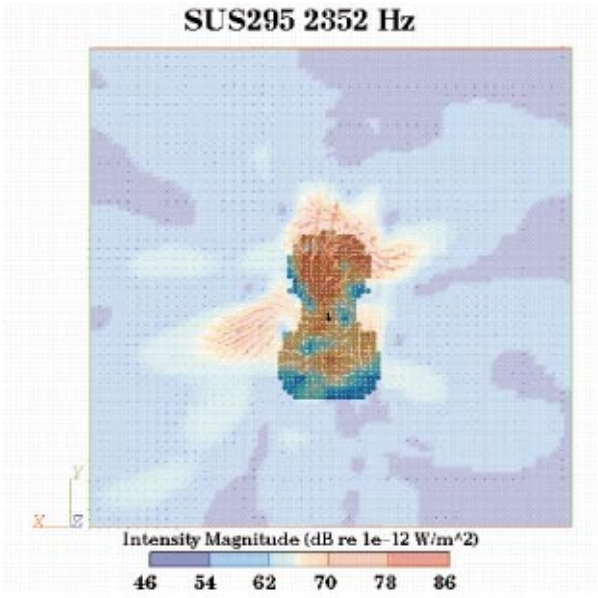

(b)

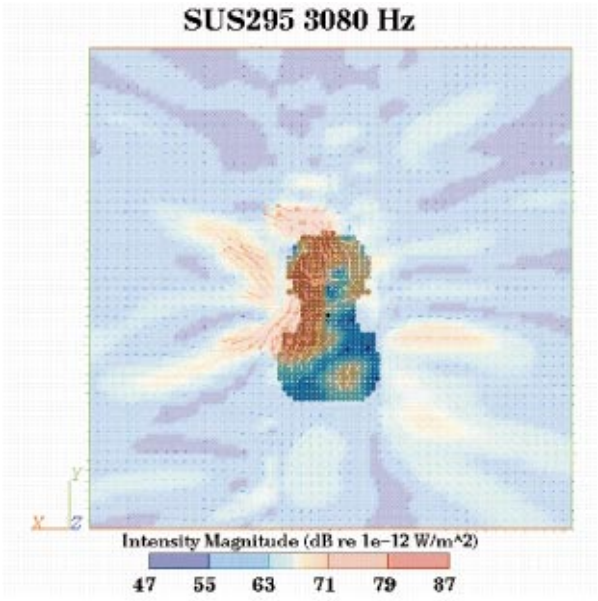

(c)

FIG. 9. Bottom edge of the back plate is rarely found to be a region of radiating energy, as evidenced by the NAH reconstructed intensity fields for violin SUS295, facing the back plate at (a) 2058 Hz, (b) 2352 Hz, and (c) 3080 Hz. The plotted data are from the closest local z plane that does not intersect the violin surface. The three-dimensional intensity vectors are shown, while the intensity vector magnitudes are denoted by color.

At 294 Hz, the *f*-hole region dominates [Fig. 3(a)], while the back plate does not display any significant sources of sound radiation [Fig. 3(b)]. This behavior corresponds to modal analysis because the first main resonance or the ''main air'' mode, which was found to be at 276 Hz for SUS295,[19] exhibits air pumping in and out of the *f* holes. The frequency of resonance for this mode is expected to shift slightly, depending on test conditions,[27] but certainly it is located close to the 294 Hz excitation. Thus, the air mode is a major contributor to the radiation at this frequency, with sound energy generated by air motion in and out of the *f*-hole region. Directivity patterns,[15] however, show omnidirectional radiation at 294 Hz. This is explained by the fact that the sound waves have long wavelengths at this frequency compared to the size of the violin, and therefore, energy is diffracted around the instrument to produce the far-field omnidirectional behavior.

At 440 Hz for SUS295, the region from which the strongest intensity vectors emanate is slightly above the *f* holes, from the wood in the upper half of the top plate, or upper bout [Fig. 4(a)]. At this frequency, the back plate shows more activity than was apparent at 294 Hz, but still less than the top plate [Fig. 4(b)]. Marshall[19] found the ''main wood'' mode, or the first bending mode with motion predominantly in the top plate, at 472 Hz. Now, instead of radiation from an air mode in which the body plays a small role, the motion of the body plays a dominant role in the radiation at 440 Hz. Thus, the source is located higher on the top plate in the wood, rather than at the *f*-hole region, and the back plate plays a greater role at 440 Hz than it did at 294 Hz. The

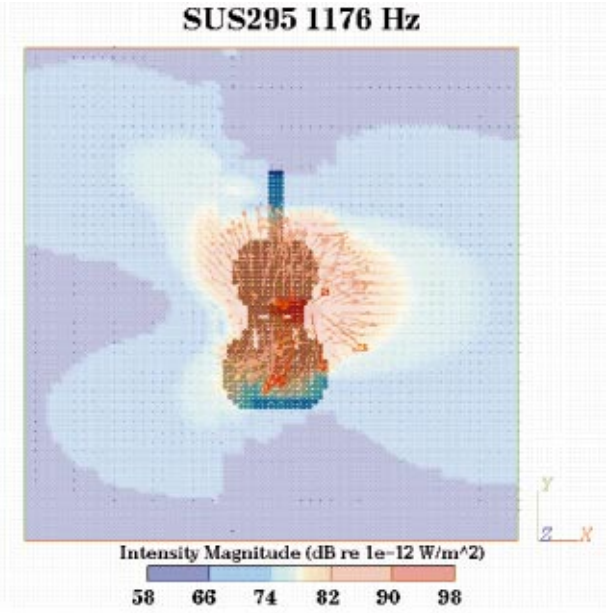

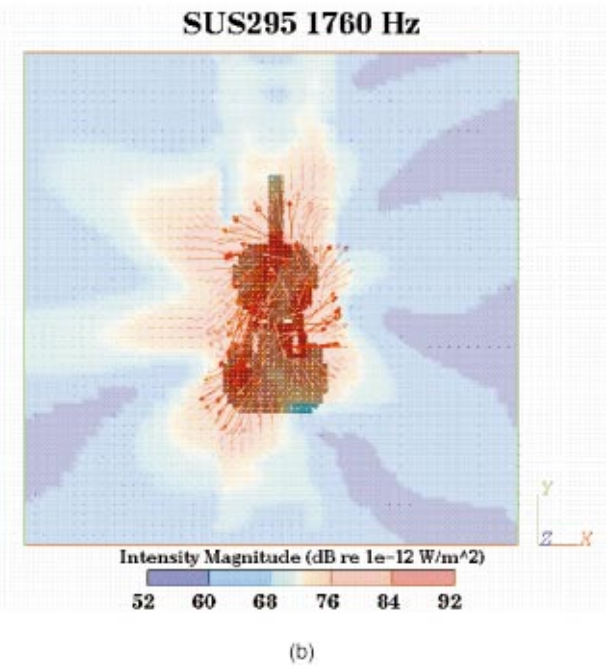

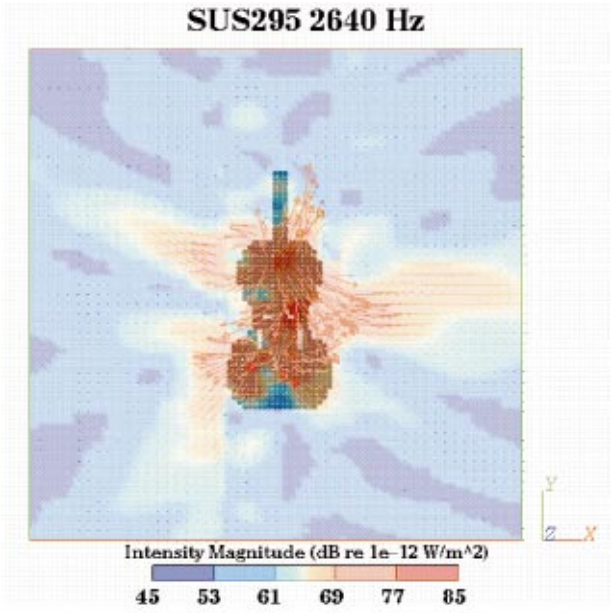

FIG. 10. Area around the soundpost is consistently a region of sound radiation activity, as supported by these NAH reconstructed intensity fields for violin SUS295, facing the top plate at (a) 1176 Hz, (b) 1760 Hz, and (c) 2640 Hz. The plotted data are from the closest local z plane that does not intersect the violin surface. The three-dimensional intensity vectors are shown, while the intensity vector magnitudes are denoted by color.

radiation mechanisms described so far for 294 and 440 Hz both correspond with modal behavior. Further comparisons of the radiation mechanisms under 1000 Hz with SUS295 mode shapes, determined from modal analysis by other researchers, are presented in Ref. 22.

The role of the violin's plates in the radiation of sound energy continues at the next lowest frequency studied of 588 Hz, which is located near a bending mode. Regions of energy radiation now appear more localized on the violin [Fig. 5(a)]. Also, some near-field effects, where the sound energy travels back towards the surface of the violin, are apparent at this frequency [Fig. 5(b)]. Overall, the radiated field at this frequency is still omnidirectional.

For the Scherl and Roth violin, the intensity vector plots at 440 Hz show similar omnidirectional results stemming primarily from the top plate. The locations of sound energy sources are not as precise, though, since the resolution is not as high as the results on SUS295. The 880 Hz intensity result for the Scherl and Roth violin similarly does not provide great detail, but it does demonstrate the predominance of the top plate in radiating sound energy and follows a cardioid radiation pattern [Figs. 6(a) and (b)], as the pressure magnitude does.[22] The cardioid pattern seems to indicate that at this frequency, the baffling effect of the violin body becomes significant, i.e., less diffraction of the radiation from the top plate occurs around the body of the violin while the sound energy propagates directly outwards from the top plate. The same cardioid shape is found in greater spatial resolution

with the SUS295 results at 880 Hz [Figs. 7(a) and (b)]. Apparently, one can summarize that at frequencies under 600 Hz, where omnidirectional radiation patterns result, the top plate is primarily responsible for radiating energy, and the sound energy diffracts around the violin, producing omnidirectional far-field results. Around the frequency 880 Hz, though, the radiation becomes baffled by the violin body, producing cardioid radiation patterns. If one assumes that the baffling begins to occur physically when ka is approximately equal to 1, where k is the acoustic wave number and a is the effective radius of the source, then for a violin a is approximately 6 cm. This corroborates theoretical estimates of $a=7$ cm by Weinreich.[28]

At frequencies above 1 kHz, the asymmetry of the violin becomes more apparent when looking at the radiation vectors emanating from the instrument (Figs. 8–10). Energy sources are more localized and distinct on the structure. Smaller source regions are expected, of course, with the shorter wavelength at higher frequencies. The asymmetry is also anticipated, since the violin is an asymmetrical instrument, due to the internal placement of the soundpost and bass bar, as well as externally with the tuning of the strings and inhomogeneities in the wood.[2] Along with the more complicated radiation mechanisms appearing above 1 kHz, the paths of the intensity vectors no longer extend directly normal to the surface of the violins, as at lower frequencies. Instead, the intensity vectors are often directed up or down into the space, mostly from the top and back plates [Fig. 8(a)]. Sometimes vectors are also found curving around the C bout and the edges of the violin, acting like line sources [Fig. 8(b)]. At frequencies below the critical frequency but above the frequencies of the lowest modes, such radiation is expected from edges of finite, unbaffled structures.

The regions of dominant sound energy radiation vary across the top and back plates for different frequencies. Two generalizations may be made, however, concerning the locations of ''hot spots.'' One is that the bottom edge of the back plate is rarely found to be a region of radiating energy [Figs. 9(a)–(c)]. Upon first glance, one may consider this to be a result of the violin mounting; however, the violin was not clamped at that location but simply held in foam at the base, and the same result is not apparent at the bottom edge of the top plate. The second trend that is noted from these studies is that the area surrounding the soundpost on the top plate consistently seems to be a region of some energy radiation [Figs. 10(a)–(c)]. The soundpost, lodged between the top and back plates, often forces vibration patterns to have a nodal point in that region. The nodal point emphasizes the violin asymmetry and leads to less cancellation of the sound field from the top plate, thereby increasing sound radiation.[29] The region around such a constraint is expected to be a source of radiating energy, as confirmed in this study.

Radiation mechanisms from the violin of different construction, Hutchins' mezzo violin SUS100, have also been characterized and compared with those discussed above for violins of standard construction, primarily SUS295. At the lowest frequency of comparison, 440 Hz, the radiated fields from both instruments are omnidirectional,[22] and the radiation mechanisms between the two instruments are also similar. The energy radiates primarily from the center region of the top plate in both instruments, while the back plate has more emphasis on the bass bar side, projecting towards the soundpost side. At the next partial, 880 Hz, it was previously noted that the two standard violins exhibit cardioid radiation patterns, with most radiation coming off of the center of the top plate leaning towards the soundpost side and more defined regions of energy radiation off the back plate which are less in magnitude [Figs. 7(a) and (b)]. The mezzo violin's behavior at this frequency is distinctly different. Although the center of the mezzo violin's top plate does radiate some

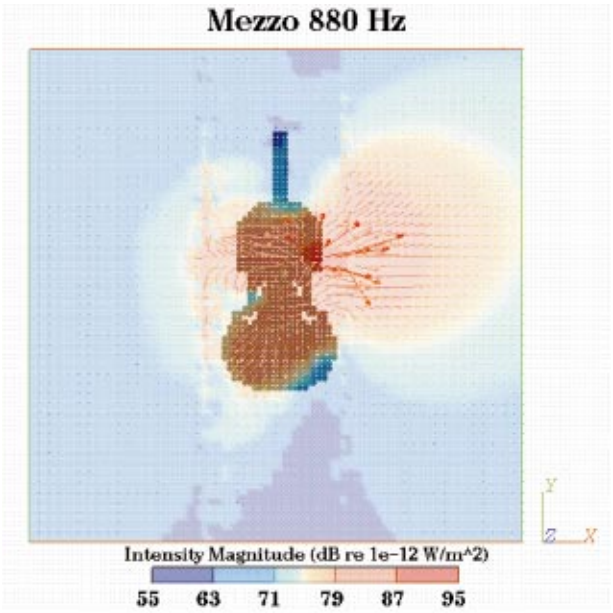

FIG. 11. NAH reconstructed intensity field for the mezzo violin SUS100 at 880 Hz: (a) facing the top plate and (b) facing the back plate. The plotted data are from the closest local z plane that does not intersect the violin surface. The three-dimensional intensity vectors are shown, while the intensity vector magnitudes are denoted by color.

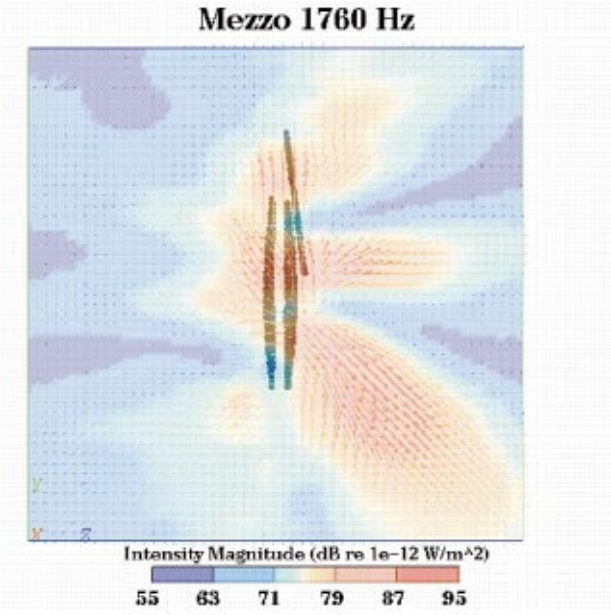

FIG. 12. NAH reconstructed intensity field for the mezzo violin SUS100 at 1760 Hz: (a) facing the bass bar side and (b) facing the top plate. The plotted data are from the closest local z plane that does not intersect the violin surface. The three-dimensional intensity vectors are shown, while the intensity vector magnitudes are denoted by color.

sound energy, the cardioid with a maximum directly normal to the top plate is not found. Instead, other regions along the soundpost side dominate the response, with the most significantly radiating area located in the upper soundpost quadrant near the upper C bout [Fig. 11(a)]. Meanwhile, the upper bass bar quadrant of the back plate shows radiating activity, as it did on SUS295, but the lower bout does not [Fig. 11(b)]. These differences may be due to differences in the modal behavior between SUS295 and the mezzo violin.[30] Unfortunately, no modal analysis data are available for the mezzo violin to assist in the analysis of the differences shown in the acoustic fields between the two violins at 880 Hz.

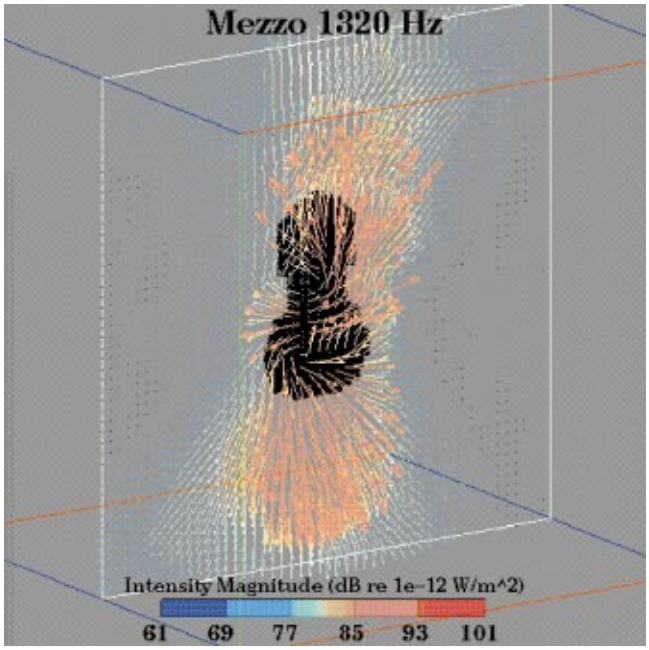

FIG. 13. Slice through the NAH reconstructed intensity vector field for the mezzo violin at 1320 Hz, showing near-field effects. The three-dimensional intensity vectors are shown, while the intensity vector magnitudes are denoted by color.

At higher frequencies, a few generalities about the mezzo violin's radiation mechanisms remain the same as for SUS295. The top plate is the dominant radiator of sound energy. Also, asymmetry is clearly apparent, with energy traveling in a variety of directions, not necessarily normal to the top plate [Fig. 12(a)]. There is evidence of near-field effects, where the sound energy from a local source turns back towards the surface, falling into a local energy sink (Fig. 13). Actual locations and the relative magnitudes of energy radiating regions differ quite significantly between the mezzo violin and the standard SUS295. However, some similarities are found between regions which do not have a large response. For example, the radiation results at 1760 Hz from the top plate of SUS295 [Fig. 10(c)] and the mezzo violin [Fig. 12(b)] both show low-intensity magnitudes in the lower soundpost quadrant.

One significant difference is apparent at the three highest frequencies studied: 2200, 2640, and 3080 Hz. Relative to the top plate's radiation, the back plate on the mezzo violin radiates much less than on the standard violin SUS295, as noted when contrasting Figs. 9(a)–(c) with Figs. 14(a) and (b). This seems rather contradictory to the instrument's purpose, since one of the main reasons for the development of the mezzo violin was to produce more sound power by increasing the area of the upper and lower quadrants. The structural changes, though, have lessened the impact of the back plate at these higher frequencies.

V. SUMMARY AND CONCLUSIONS

Regions responsible for sound energy radiation from bowed violins have been characterized for frequencies from

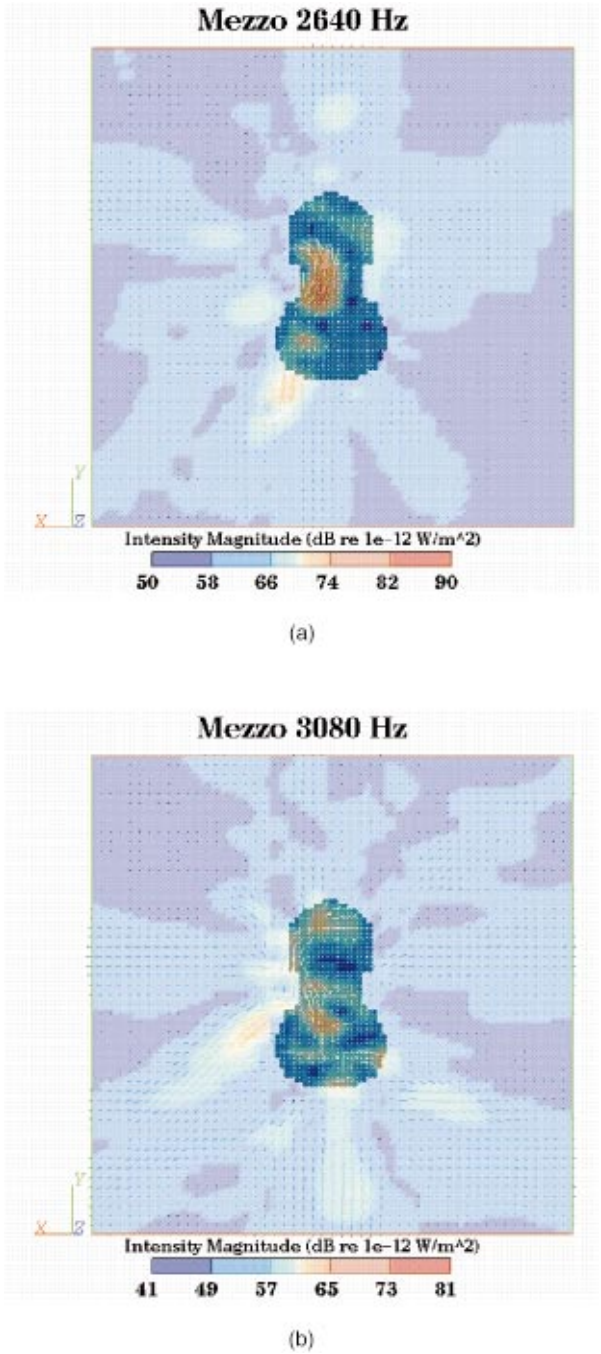

FIG. 14. NAH reconstructed intensity field for the mezzo violin SUS100 facing the back plate at (a) 2640 Hz and (b) 3080 Hz. The plotted data are from the closest local z plane that does not intersect the violin surface. The three-dimensional intensity vectors are shown, while the intensity vector magnitudes are denoted by color.

294 Hz to 3 kHz, by applying multiplanar NAH. Certain trends in the sound energy radiation across frequencies were noted. First, the top plate was found to be the dominant source of sound energy radiation from the violins. At low frequencies, diffraction of sound radiation from the top plate around the violin body produces far-field omnidirectional radiation. Around 880 Hz, baffling by the violin body begins to produce far-field cardioid patterns since the energy is radiating primarily from the top plate. At higher frequencies, the regions of energy sources become more localized and are distributed asymmetrically on the violin body. Evidence shows that sound radiation rarely originates from the bottom edge of the back plate, but often radiation is found stemming from the area around the soundpost of the top plate.

The significant conclusions of these results are varied. Because of the clear dominance of the violin's top plate in sound energy production, the tuning of the top plate may be more crucial than that of the back plate during violin construction, in terms of the instrument's strength. The fact that the violin top plate faces out towards the audience in performance indicates an intuitive understanding over time of where most of the sound energy comes from, and this study has confirmed it. Additionally, the long-standing belief among violin makers and players that the placement of the soundpost critically affects an instrument's sound is justified, since the soundpost region has been found to be a predominant source region at most of the frequencies studied.

Comparison of results between the three violins has indicated similarities between the two violins of normal construction, but significant differences with the mezzo violin. The mezzo violin results do demonstrate similar general trends across frequencies, namely, that the top plate is the main radiator. However, the mezzo violin's back plate plays a more minor role relative to the top plate at frequencies between 2 and 3 kHz than is true for standard violins. It appears that the coupling to the back plate is reduced in the mezzo violin, perhaps due to the combination of thinner ribs and greater back plate area across which to transmit the vibrational energy. The lesser amount of sound radiation from the back plate may not affect the overall sound level from the violin which reaches the audience; indeed, there is evidence that the mezzo violin is more powerful than ordinary violins at certain low frequencies.[22] However, the lack of back plate radiation may affect how the instrument is subjectively experienced by the player.

ACKNOWLEDGMENTS

The authors are grateful to Carleen Hutchins for the loan of her violins, SUS295 and SUS100. This work has been supported by a National Science Foundation (NSF) Graduate Research Fellowship, American Association for Women (AAUW) Selected Dissertations Fellowship, and a Bell Laboratories Graduate Research Program for Women (GRPW) grant.

[1] J. A. Moral and E. V. Jansson, ''Eigenmodes, input admittance, and the function of the violin,'' Acustica **50**, 329–337 (1982).
[2] K. D. Marshall, '''Modal analysis of a violin,'' J. Acoust. Soc. Am. **77**, 695–709 (1985).
[3] E. V. Jansson, N. E. Molin, and H. O. Saldner, ''On eigenmodes of the violin—Electronic holography and admittance measurements,'' J. Acoust. Soc. Am. **95**, 1100–1105 (1994).
[4] F. A. Saunders, ''The mechanical action of violins,'' J. Acoust. Soc. Am. **9**, 91–98 (1937).
[5] E. V. Jansson, ''Long-time-average spectra applied to analysis of music. Part III: A simple method for surveyable analysis of complex sound sources by means of a reverberation chamber,'' Acustica **34**, 275–280 (1976).
[6] A. Gabrielsson and E. V. Jansson, ''Long-time-average spectra and rated qualities of twenty-two violins,'' Acustica **42**, 47–55 (1979).
[7] J. Tro, O. Kr. Ø. Pettersen, and U. K. Kristiansen, ''Sound radiation from a double bass visualized by intensity vectors,'' J. Catgut Acoust. Soc. **40**, 7–9 (1983).

[8] H. Tachibana, H. Yano, and Y. Hidaka, ''Visualization of sound fields by the sound intensity technique,'' Proceedings of the 2nd Symposium on Acoustic Intensity, Tokyo, Japan, pp. 117–126 (1988) (in Japanese).
[9] G. Weinreich and E. B. Arnold, ''Method for measuring acoustic radiation fields,'' J. Acoust. Soc. Am. **68**, 404–411 (1980).
[10] E. G. Williams, J. D. Maynard, and E. Skudrzyk, ''Sound source reconstructions using a microphone array,'' J. Acoust. Soc. Am. **68**, 340–344 (1980).
[11] J. D. Maynard, E. G. Williams, and Y. Lee, ''Near-field acoustic holography: I. Theory of generalized holography and the development of NAH,'' J. Acoust. Soc. Am. **78**, 1395–1413 (1985).
[12] W. Y. Strong, Jr., T. B. Beyer, D. J. Bowen, E. G. Williams, and J. D. Maynard, ''Studying a guitar's radiation properties with near-field holography,'' J. Guitar Acoustics **6**, 50–59 (1982).
[13] W. Y. Strong, Jr., E. Torick, and J. D. Maynard, ''Experimental study of vibration and radiation characteristics of a violin,'' J. Acoust. Soc. Am. **72**, S83 (1982).
[14] C. M. Hutchins and J. C. Schelling, ''A new concert violin,'' J. Audio Eng. Soc. **15**, 432–436 (1967).
[15] L. M. Wang and C. B. Burroughs, ''Directivity patterns of acoustic radiation from bowed violins,'' J. Catgut Acoust. Soc. **3**, 7–15 (1999).
[16] H. Dünnwald, ''Deduction of objective quality parameters on old and new violins,'' J. Catgut Acoust. Soc. **1**, 1–5 (1991).
[17] G. Bissinger, ''Some mechanical and acoustical consequences of the violin soundpost,'' J. Acoust. Soc. Am. **97**, 3154–3164 (1995).
[18] G. Bissinger, ''Modeling the sound of the violin: The V–R model and the role of the soundpost,'' J. Catgut Acoust. Soc. **3**, 29–37 (1998).
[19] K. D. Marshall, personal research notes (1990).
[20] O. E. Rodgers, ''Effect on plate frequencies of local wood removal from violin plates supported at the edges,'' J. Catgut Acoust. Soc. **1**, 7–11 (1991).
[21] O. E. Rodgers, private communications (1997).
[22] L. M. Wang, ''Radiation mechanisms from bowed violins,'' Ph.D., Pennsylvania State University (1999).
[23] C. M. Hutchins, ''A 30-year experiment in the acoustical and musical development of violin-family instruments,'' J. Acoust. Soc. Am. **92**, 639–650 (1992).
[24] A. Askenfelt, ''Measurement of bow motion and bow force in violin playing,'' J. Acoust. Soc. Am. **80**, 1007–1015 (1986).
[25] A. Askenfelt, ''Measurement of the bowing parameters in violin playing. II: Bow–bridge distance, dynamic range, and limits of bow force,'' J. Acoust. Soc. Am. **86**, 503–516 (1989).
[26] E. G. Williams, *Fourier Acoustics: Sound Radiation and Near-Field Acoustical Holography* (Academic Press, San Diego, CA, 1999), p. 105.
[27] M. Roberts and T. D. Rossing, ''Normal modes of vibration in violins,'' J. Catgut Acoust. Soc. **3**, 3–9 (1998).
[28] G. Weinreich, ''Directional tone color,'' J. Acoust. Soc. Am. **101**, 2338–2346 (1997).
[29] C. M. Hutchins, ''A history of violin research,'' J. Acoust. Soc. Am. **73**, 1421–1440 (1983).
[30] Admittance plots for SUS295 and the mezzo violin SUS100 are distinctly different in the low-frequency regime, as shown in Ref. 22, implying different modal behavior.